DOI: 10.1021/cg1015548

CRYSTAL GROWTH & DESIGN Article

2011, Vol. 11
320–327

A Real Time Microscopy Study of the Growth of Giant Au Microplates

B. Radha and G. U. Kulkarni*

Chemistry and Physics of Materials Unit and DST Unit on Nanoscience, Jawaharlal Nehru Centre for Advanced Scientific Research, Jakkur P.O., Bangalore 560064, India

Received October 8, 2010

Ⓦ This paper contains enhanced objects available on the Internet at http://pubs.acs.org/crystal.

ABSTRACT: A simple air-thermolysis of a precursor, $(AuCl_4)^-$ phase transferred from aqueous medium and stabilized in toluene by tetraoctylammonium bromide (ToABr), is found to yield unusually large ($\sim$12 000 μm^2) hexagonal and triangular Au microplates. The optimal conditions for the growth of microplates with edge lengths over 100 μm are $(AuCl_4)^-$/ToABr ratio of 1:4.4 for phase transfer and thermolysis on a flat substrate such as Si at 130 °C for 24 h. Scanning electron microscopy performed using a heated stage showed nucleation of nanoparticles into dendrimeric structures and rudimentary shapes, which took several minutes to anneal into well-formed single crystalline triangles and hexagons. Amazingly quite often the plates were held vertical to the substrate surface during the growth even at large sizes, as evidenced by in situ optical microscopy. Three growth modes, namely, nucleation of tiny nanoparticles into dendrimeric structures which assemble into specific shapes, atom-by-atom addition from the precursor feedstock, and fusion of three-dimensional particles to the growing microplates, have been inferred from this study using real time microscopy.

Introduction

Anisotropic metal nanostructures form an interesting area of research[1] with potentially important applications in diverse fields such as catalysis,[2] multicolor diagnostics,[3] and optoelectronics.[4] An anisotropic structure is almost anything that is not even approximately spherical, obvious examples being prismatic[5] and elongated nanoparticles (the latter also known as nanorods), triangular[6] and hexagonal[7] plate-like structures, decahedra, icosahedra, and truncated tetrahedral structures.[8] Other structures include nanobelts,[9] tetrahexahedral nanocrystals,[10] rice-shaped particles,[11] pentagonal bipyramidal,[12] and star-shaped particles.[13] While the literature in the last decade is abundant with reports on the synthesis and properties of such anisotropic structures, aspects related to growth are still being actively pursued.[14] It has been our interest to investigate how from tiny nuclei plate-like structures in definite shapes emerge. Employing in situ X-ray absorption fine structure (XAFS) and optical measurements, Murayama et al. evidenced the growth of Ag triangular nanoplates as the aggregation of small spherical nanoparticles.[15] UV−vis absorption spectroscopy has also been used.[16] The anisotropy of the growing particle expresses itself as increasing absorption at longer wavelengths due to longitudinal plasmon. From total energy calculations, it is proposed that the energy required to build larger anisotropic structures could be less than the one required to build isotropic structures.[17] Several growth studies have been carried out ex situ by arresting the growth at intermediate stages. The spontaneous transformation process of aggregated nanoparticles to triangular and hexagonal nanocrystals confined by a dendrimeric structure has been reported.[18] Seed formation followed by fusion of aggregates and recrystallization leading to Au nanoplate formation has been observed.[7] In the case of nanobelts, it was observed that nanotriangles assemble in a one-dimensional (1D) manner and recrystallize to form single-crystalline nanobelts.[9] Small nanoplates connecting together along the {110} lateral planes produce large hexagonal and triangular nanoplates which was confirmed using transmission electron microscopy (TEM) analysis.[19] On the basis of the above studies, it may be stated that where organic moieties are part of the synthetic process, their preferential adsorption to specific nanocrystal surface sites or facets may poison or accelerate the addition of fresh adatoms thus inducing anisotropy. Such restrictions may also occur in micellar organization formed by surfactants. Another factor responsible for anisotropic growth is the presence of twin planes in the nanocrystal.[14] Using TEM analysis, Yang et al. have shown that a grain-rotation-induced coalescence mechanism is at play for filling in nanopores present in growing Au nanoplates.[20]

In a recent study involving a Au-organic precursor, we obtained by simple thermolysis in air, large hexagonal and triangular Au microplates and reported their utility as platforms for live cells.[21] Obviously, these structures have been highly anisotropic, perhaps among the most anisotropic large structures. Importantly, we have observed that the growth took place over several minutes to hours which prompted and enabled us to do a detailed investigation of the growth itself. Previous studies on growth of Au microplates have all been carried out in the solution phase,[7,10,18,19] and these plates are typically a few hundred nanometers to a few micrometers. Here we report the real time imaging of the growth of plates on solid substrates from nanometer size to a few tens of micrometers using high resolution scanning electron microscopy and optical microscopy. The growth could be slowed down to several hours simply by reducing the thermolysis temperature to just above the solvent evaporation temperature.

Experimental Section

Hydrogen tetrachloroaurate(III) hydrate, tetraoctylammonium bromide (ToABr), and toluene were obtained from Sigma Aldrich and used without further purification. The water used throughout this investigation was double distilled and deionized. The precursor for microplate synthesis is essentially a complex containing $(AuCl_4)^-$

*Author to whom correspondence should be addressed. Telephone: +91-80-2208 2814. Fax: +91-80-2208 2766. E-mail: kulkarni@jncasr.ac.in.

 Published on Web 12/17/2010

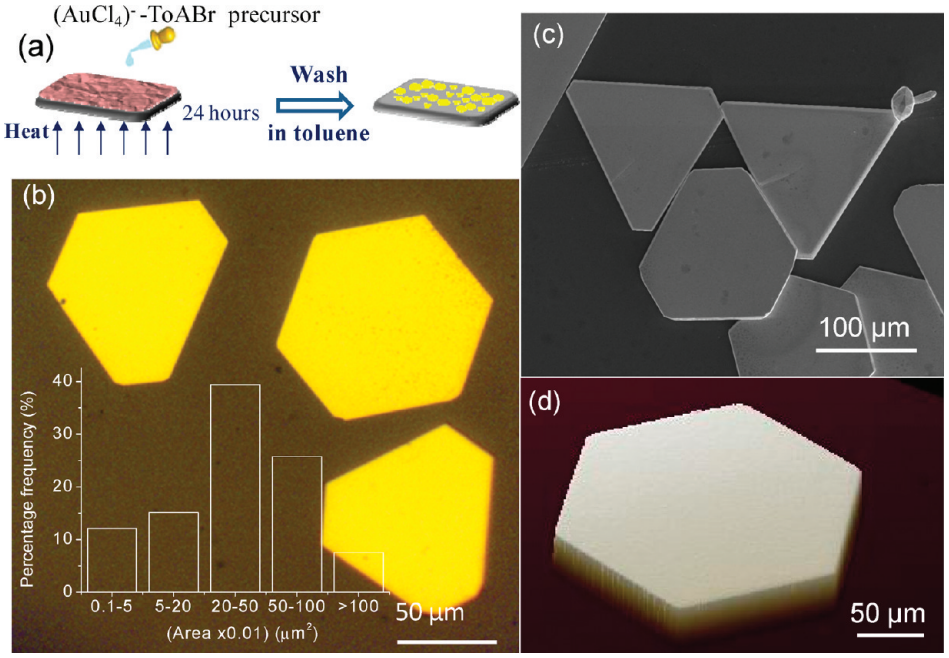

Figure 1. (a) Schematic showing the procedure for making Au microplates. The $(AuCl_4)^-$-ToABr precursor solution is drop coated onto a given substrate and then thermolyzed at 130 °C for 24 h. (b) Optical image of the microplates with an overlay of a histogram of the plate area, (c) a low magnification SEM image of microplates and (d) optical profilometric image showing the smooth surface of a Au hexagon.

ions stabilized in ToABr (25 mM in toluene), termed $(AuCl_4)^-$-ToABr. It was prepared following a literature procedure.[22] Briefly, the precursor was prepared by phase transfer of $(AuCl_4)^-$ ions from an aqueous solution (25 mmol/L, 3.2 mL) to toluene (8 mL) using ToABr (50 mmol/L) as a phase transfer agent. This corresponds to a $(AuCl_4)^-$ to ToABr ratio of 1:4.4. Likewise, the phase transfer was carried out with varying ratios of $(AuCl_4)^-$ and ToABr (1:1 to 1:8.8). The two-phase mixture was vigorously stirred until all the $(AuCl_4)^-$ ions were transferred into the organic layer. As the phase transfer proceeded, the yellow colored bottom aqueous layer became colorless and the top organic layer developed a red color. The organic layer was separated and drop coated onto the chosen substrate. Thermolysis was carried out in air at 130 °C for up to 24 h. Thermal treatment was found to be more effective in producing the microplates than using external reducing or stabilizing agents; the latter only led to nanoparticle formation, as is well-known from the literature as well.[22] Following thermolysis, a gentle wash in toluene was carried out to remove any remaining precursor. Different substrates have been tried out - Si, glass, stainless steel, mica or HOPG, and flexible substrates such as polyimide, polydimethylsiloxane - almost any smooth surface that can stand temperature and remain insoluble in the solvent should serve this purpose (Supporting Information, Figure S1). The resulting Au microplates were examined using an optical microscope (Laben, India) and a Wyko NT1100 optical profiler (Veeco, USA). Field emission scanning electron microscopy (FESEM) images were obtained using a Nova NanoSEM 600 instrument, FEI Co., The Netherlands. For TEM microscopy, microplates were dispersed in toluene and a drop was placed on a holey carbon grid. This grid was used for TEM and selected area electron diffraction (SAED) analysis in a JEOL-3010 instrument operating at 300 kV. X-ray diffraction (XRD) measurements were performed using a Siemens Seifert 3000TT diffractometer (Cu Kα 1.5406 Å, scan rate, 0.5° min^{-1}). Fourier transform infrared measurements (FTIR) were done using a Bruker IFS66v/s spectrometer with a resolution of 2 cm^{-1}. Thermogravimetric analysis (TGA) was carried out using a Mettler Toledo, TG-850 set in the temperature range of 30−300 °C at a heating rate of 3 °C/min in N_2 atmosphere. The $(AuCl_4)^-$-ToABr precursor was taken in the form of solid (total weight, 10.9 mg) in a porcelain boat.

Results and Discussion

$(AuCl_4)^-$-ToABr is a crystalline molecular solid complex, as shown by XRD data (see Supporing information, Figure S2). The reaction is essentially unaided by any solvent (Figure 1a). The thermolysis process initially melts the precursor (mp 85 °C) and brings about the reduction of Au(III) to Au(I) initially by the formation of colorless $AuBr_2^-$ (for similar observations, see ref 23), followed by the reduction of Au(I) to Au(0), which typically goes on for several hours. The reduced gold was found to be mostly in the form of microplates. The optical microscopy images of a few typical triangular and hexagonal microplates, on glass substrate are shown in Figure 1b. The edge lengths of the plates are seen to extend to several tens of micrometers. As shown in the histogram in Figure 1b, microplates with areas 5000−10 000 μm^2 were commonly seen. The thickness was more frequently sub-μm (Supporting Information, Figure S3). Figure 1c shows a typical FESEM image with several microplates covering a Si substrate; very few particulates are seen in the image. Importantly, the plates maintain smoothness (~1 nm) over large areas as revealed by optical profilometry (Figure 1d and Supporting Information, Figure S4). The plates are highly reflective and metallic. The UV−visible absorption spectrum of the formed microplates is shown in Figure S5, Supporting Information.

The process of transformation of Au(III) to Au(0) to form microplates was followed by in situ FTIR and TGA measurements (Figure 2). Prior to thermolysis, the room temperature FTIR spectrum of $(AuCl_4)^-$-ToABr displays characteristic C−H stretches of the methylene and the end methyl groups of the alkane chain in the 2800−3000 cm^{-1} region (Figure 2a). The symmetric and antisymmetric methylene C−H stretches appear around 2851 and 2920 cm^{-1}. The methyl symmetric and antisymmetric stretches are centered around 2875 and 2953 cm^{-1}. As the thermolysis progresses above 130 °C, these peaks seem to shift upwardly by at least 4 cm^{-1}. This is the possible existence of defects in alkane chains[24] at elevated temperatures. The FTIR spectrum at 250 °C is featureless, indicating perhaps complete metallization. At 250 °C, the residual weight (10.4%) in TGA data nearly corresponds to

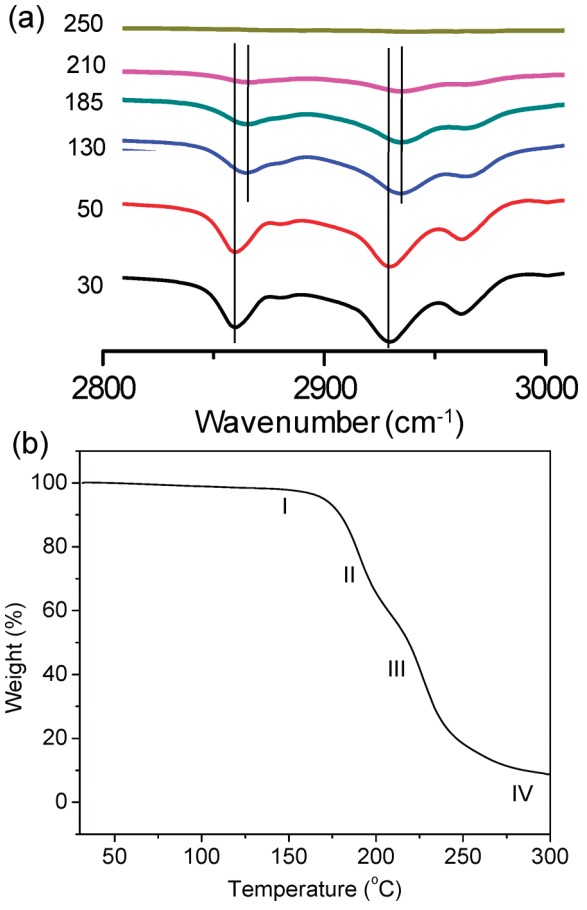

Figure 2. (a) In-situ FTIR spectra of the $(AuCl_4)^-$-ToABr precursor subjected to thermolysis in air at various temperatures. (b) Thermogravimetric analysis of the precursor prepared with $(AuCl_4)^-$ and ToABr ratio of 1:4.4. The weight loss in TGA occurs in four steps - region I (5.04%), regions II (51.2%), region III (33.25%), and region IV (10.4%) correspond respectively to the solvent evaporation, decomposition, and desorption of ToABr, ToA, and chloride ions, and the metallic residue.

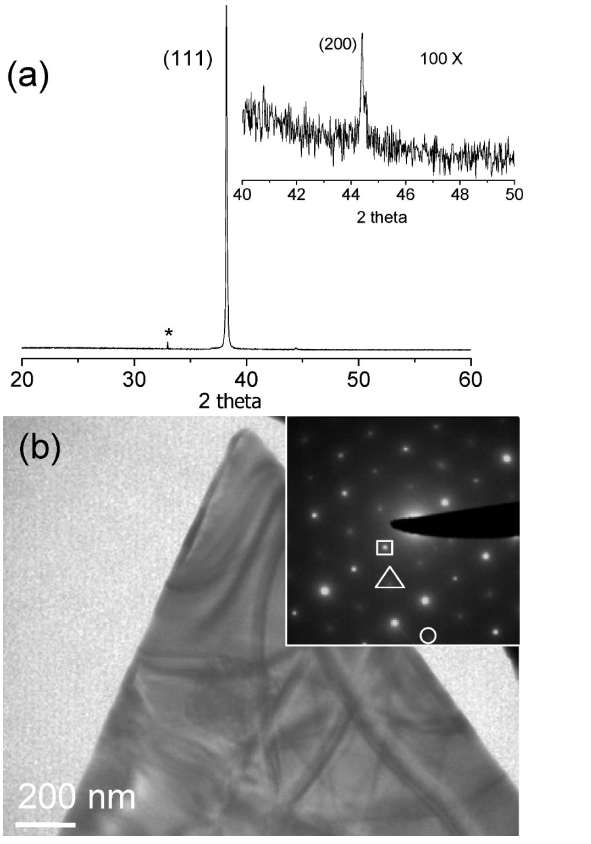

Figure 3. (a) XRD pattern of the thermolyzed Au-ToABr with the peaks matching with the JCPDS (PDF No. 040784), * corresponds to a peak from the Si substrate. The inset shows the (200) peak with its intensity multiplied by 100 times. (b) TEM image of a triangular microplate, with the SAED pattern shown as inset. Square, triangle, and circle correspond to {220}, {422}, {440} planes, respectively.

the Au content in the complex with no residual from the hydrocarbon. This is essentially a complete removal of ToABr. If the residue of 10.4% in TGA (see region IV in Figure 2b) is taken to be the metallic species, the starting precursor would correspond to $N^+(C_8H_{17})_4AuCl_4^- \cdot 2N(C_8H_{17})_4Br$ (molecular weight, 1899.25). This is somewhat less compared to the starting ratio (1:4.4); some loss of ToABr units is expected at the aqueous−organic interface.

Figure 3a shows the powder XRD pattern from a film of $(AuCl_4)^-$-ToABr precursor thermolyzed at 250 °C for 30 min. The peaks in XRD could be indexed to the standard face centered cubic (FCC) crystalline structure of Au (a = 4.078, JCPDS PDF No. 040784). There is essentially one intense sharp peak assignable to (111), indicating the high purity and single phase nature of the sample. Furthermore, the relative diffraction intensity of (111) to (200) is 100:0.02, which is much lower than the corresponding value from bulk gold (100:52, JCPDS PDF No. 040784). Figure 3b shows TEM image of a truncated triangular plate. The contours seen in the image originate from the diffraction effects arising due to slight bending of the thin plate on the TEM grid surface.[19] The SAED pattern shown in the inset is hexagonally symmetric and corresponds to Au (FCC) crystalline lattice viewed along the ⟨111⟩ direction. The spots representing {220}, {422}, {440} bragg planes are clearly visible. Importantly, we do not see any kinematically forbidden spots such as 1/3{422}, attributed to the presence of two or more twin planes in the nanoplates.[25]

The effect of varying the ratio, $(AuCl_4)^-$ to ToABr, during the preparation of the precursor for Au microplates has been examined. As the ToABr proportion in the precursor increased from being 1:1, the edge lengths of the resulting microplates increase (Figure 4a). The ratio of 1:4.4 for $(AuCl_4)^-$/ToABr proves to be the most effective to yield large microplates at 130 °C (see Figure 1). A further increase in the ToABr content makes the overall Au content less and the resulting microplates have reduced sizes. The effect of thermolysis temperature was also examined. As shown in Figure 4b, large edge lengths are found with 130 °C treatment. With the increase in the thermolysis temperature, the decomposition kinetics is expected to be faster, influencing adversely the growth of the plates. Thus, at elevated temperatures, small-sized plates are obtained along with Au nanoparticles. Below 130 °C, the decomposition of $(AuCl_4)^-$-ToABr does not seem possible at all.

The growth of Au nanostructures was monitored in situ at 130 °C in the FESEM chamber. Within 5 min, nanoparticles were seen nucleating to form dendrimeric structures (see Movie 1 and also Figure 5a−c). Interestingly, these are essentially rudimentary shapes of triangles and hexagons. After 15 min, the nanoparticles fused to form well-defined shapes (Figure 5d). As the structures grew, a halo was commonly seen surrounding the structures, corresponding to the metal

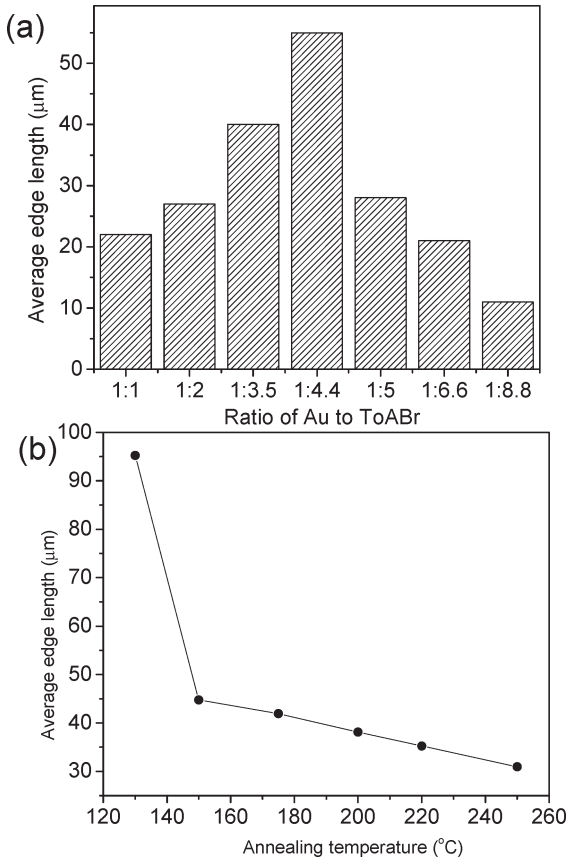

Figure 4. (a) A histogram of the average edge length of microplates obtained with different $(AuCl_4)^-$/ToABr ratios (thermolysis conditions, 130 °C, 6 h). (b) Variation in the average edge length with respect to the thermolysis temperature. The ratio chosen for the precursor synthesis was 1:4.4. Temperature ramp, 2 °C/min, and thermolysis time was 24 h.

precursor in its molten state (melting point 85 °C). This formed a feedstock of Au atoms for the growing structures. Besides the structures shown, bigger particles with 3D shapes such as prismatic and dodecahedral were also seen occasionally.

During further growth, there is a competition between the platelike structures and particles with 3D shapes. It is seen from the various examples shown in Figure 6 where the 3D particles are connected to corners and edges of triangular and hexagonal microplates. On the basis of this observation, one may speculate that the 3D structures dissolve away and merge with the microplates as the plates represent the lowest surface energy (111) plane[26] against which the higher surface energy structures are sacrificed. Accordingly, the 3D structures are rarely seen in the final product obtained after extended thermolysis.

We have seen something very interesting under the optical microscope, for the first time in the literature. As growth continues at a large length scale, a number of tiny microplates were seen all over, often vertical to the substrate. In Figure 7a, a few microplates are seen brightly reflecting (marked 1−5) and these must be lying flat. There are other plates (6−10), which appear as elongated rodlike structures. A careful observation of the structures marked 11−15 in Figure 7a reveals that these microplates are standing vertical to the substrate but slightly slanted. Indeed, the rodlike appearing structures with darker contrast (6−10) are also microplates standing vertically. The vertically standing microplates are seen more

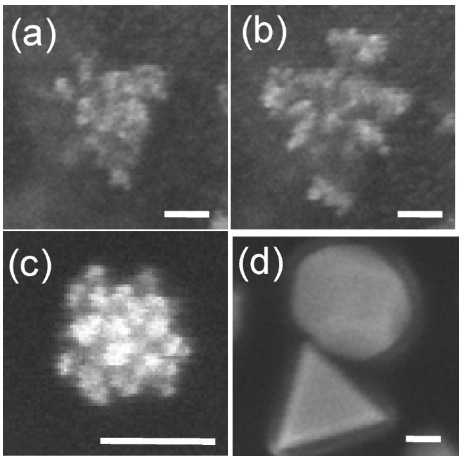

Figure 5. SEM images: (a, b) Initiation of dendrimeric growth and triangular shapes emerging from aggregation, (c) a hexagonal shape, (d) the fusion of nanoparticles is near complete to form a well-defined triangle. Panel (b) is the image taken of the same triangular aggregation as in (a) after 60 s. The halo seen around the particles in (d) represents the $(AuCl_4)^-$-ToABr feedstock. Scale bar corresponds to 100 nm.

clearly in the SEM image shown in Figure 7b. It is observed that the initial growth of the Au microplates (60−70%) happens vertically to the substrate, which was monitored in real time employing in situ optical microscopy (see Movie 2). After certain growth, the microplates fall off flat to the substrate, as the feedstock surrounding them gets depleted.

Most often, the growth of the Au plates takes place in the molten precursor feedstock as described above. In some cases, we observed the liquid front moving away, with microplates staying outside (see Movie 3). In the following stages, we observed dendrimeric offshoots as if originating from the vertices. As seen in Figure 8, the particulate structures established a connection with the microplate in the course of time. These dendrimeric connections are more clearly visualized in the SEM image as shown in the inset taking the example of a different microplate.

The dimensions of the growing plates were noted using optical microscopy (Figure 9), taking both hexagonal and triangular shapes as case examples. At 130 °C (Figure 9a), the areas of the microplates are seen to increase linearly with the time of annealing, which essentially translates to a linear dimension going as the square root of growth time. Thus, it implies that the growth is diffusion limited,[27] especially at sizes relevant to optical microscopy. Indeed, this is the first experimental observation of diffusion limited growth of an anisotropic structure at such a large length scale. Of course, the slope of the growth curve can be different for different plates with different shapes (see Figure 9a), although no systematic dependence can be expected based on shape alone. For the examples chosen in Figure 9, the triangles outscore the hexagons in terms of slope. Among many parameters at play (which is unclear to us at present), the slope should depend on the local concentration of the precursor and the annealing temperature. At 180 °C, the growth of the microplates was in general faster as also seen in the case of plates shown in Figure 9b, although the ultimate sizes attained were much larger at 130 °C (see Figure 1). It is also commonly observed that in the case of triangular microplates, the corners get rounded after a while and further growth actually led to the truncation of the triangles (see images shown in Figure 9).

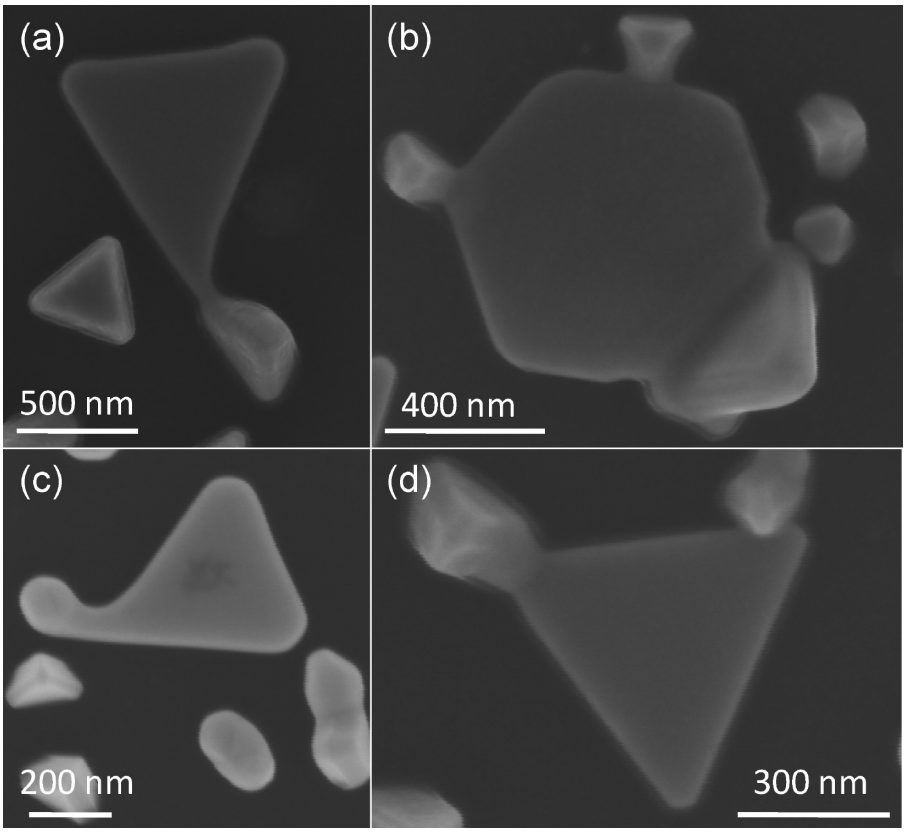

Figure 6. (a−d) 3D Au nanostructures sacrificing to merge with the 2D nanoplates.

This is reflected in the slope of the growth curve. Perhaps an increase in the perimeter because of truncation leads to a faster growth (see Figure 9) as there is increased interface between the growing plate and the precursor feedstock. Thus, many truncated triangular or asymmetric hexagonal microplates are commonly seen (see Figure 1).

From the above observations, at least three different modes of growth, not necessarily sequential, may be identified, namely, the nucleation of tiny nanoparticles into dendrimeric structures which assemble into specific shapes,[18] atom-by-atom addition to the formed platelets[7] from the precursor feedstock, and fusion of the 3D particles to growing microplates.[28] While all the three modes are found in the literature reports, their occurrences in the present study deserve some mention (see schematic diagram in Figure 10). Ours is not a solution-based method but more like a solid state synthesis. The reaction is essentially unaided by any solvent. Moreover, the precursor is highly enriched with Au (10 wt %) and the thermolysis product is reduced metal with hardly any trace of impurities. The microplate growth condition is such that the temperature is just above the solvent boiling point at which the precursor remains in the molten state (mp 85 °C). A modest temperature of 130 °C can slow down the kinetics (see Figure 2b for the decomposition steps), ideally suited for ultraslow growth of Au nanostructures amidst the molten precursor. A slow growth is expected to induce high anisotropy as well as well-formed facets in the obtained structures.[29] The nucleation of nanoparticles takes place in this feedstock and leads to dendrimeric structures. As the nanoparticles come together while afloat in the liquid feedstock with facets guiding their orientations, they anneal themselves into definite shapes (mostly triangular or hexagonal) amidst the fluidic precursor. Once a well-annealed anisotropic structure starts emerging, its growth is entirely dependent on atom-by-atom addition from the fluidic precursor (see Figure 10) with no addition of nanoparticles. Such a distinct stage of atom-by-atom addition has not been commonly observed.[7,28] Further growth of the microplate can also take place by the addition of 3D nanoparticles. We have thus realized that such a slow reaction kinetics is possible with $(AuCl_4)^-$-ToABr complex, leading to Au microplates formation[29] rather than spherical particles. We have done the variation of alkyl chain length in tetraalkylammonium bromide to study the effect on the growth. Tetraoctylammonium bromide gives the largest Au microplates among all (see Supporting Information, Table S1).

In an effort to throw more light on the proposed mechanism, we have performed thermal studies on the Au microplates. If the microplates were to form by the fusion of tiny platelets, it is reasonable to expect that they would disintegrate into particles.[30] But what we have seen is something very different. In the present study, when the Au microplates were annealed at 350 °C for longer time (6 h), microplates do defragment, but the mode of defragmentation is found to be quite different from that was observed previously (see ref 30). In the examples shown in Figure 11, it is clear that the metal has flown outwardly thinning the middle region and in some cases even rupturing to form holes near the vertices. We have understood this process as follows. A fully grown microplate is essentially a well-annealed single crystal with little defects. When subjected to higher temperatures (350 °C) on a hot plate (Figure 11), the middle region of the microplates melts readily as expected due to restricted heat flow, and as a result the metal flows outwardly making the polygons appear thicker at

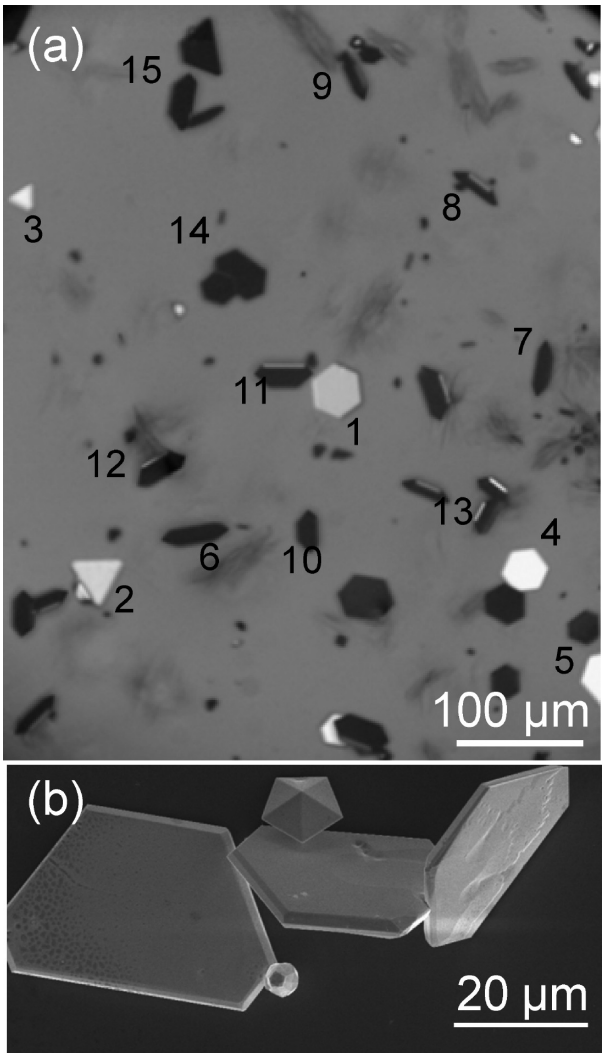

Figure 7. (a) Optical image of a region showing many vertical (marked 6−15) Au microplates along with a few plates lying flat (1−5). (b) SEM image of three microplates which are slanted and vertical to the substrate. Two 3D particles with pentagonal prismatic and dodecahedral shapes are also seen.

the edges. This effect is more pronounced at the vertices (Figure 11a,d). If the vertices are closer as in the case of truncated triangular plates, this leads to a crack (Figure 11b,e). The propagation of this crack creates interesting shapes as shown in Figure 11c,f. For the microplates reported in the literature, elevated temperatures cause cracking and degeneration.[30] For such plates formed by particle fusion, the presence of impurities along particle boundaries (from reagents used in the synthetic process) can lead to breaking up of the microplate into particulate islands, from which the microplate had formed.

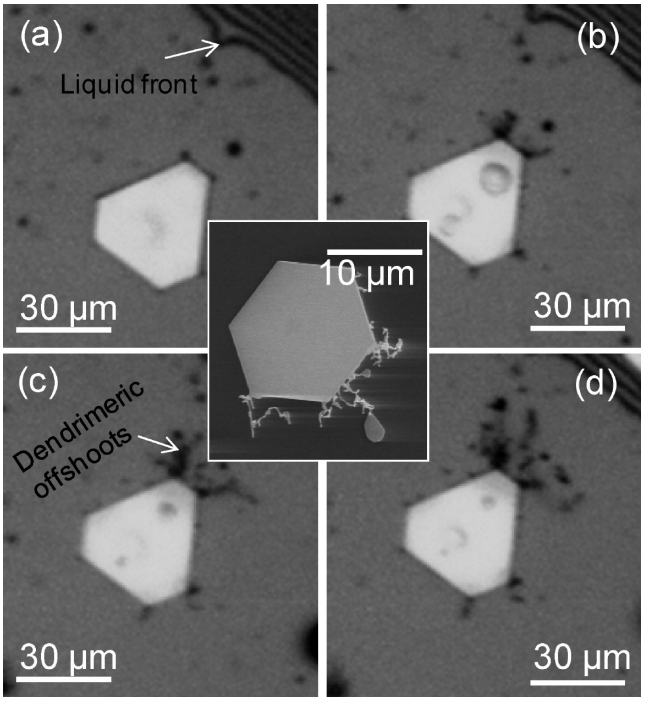

Figure 8. Ⓦ Optical images of a Au microplate lying just outside of the precursor feedstock captured at successive intervals, (a) 30 min, (b) 40 min, (c) 50 min, and (d) 60 min (also see Movie 3). Inset shows the SEM image of a hexagonal Au microplate under similar conditions where the growth was stopped at an intermediate stage.

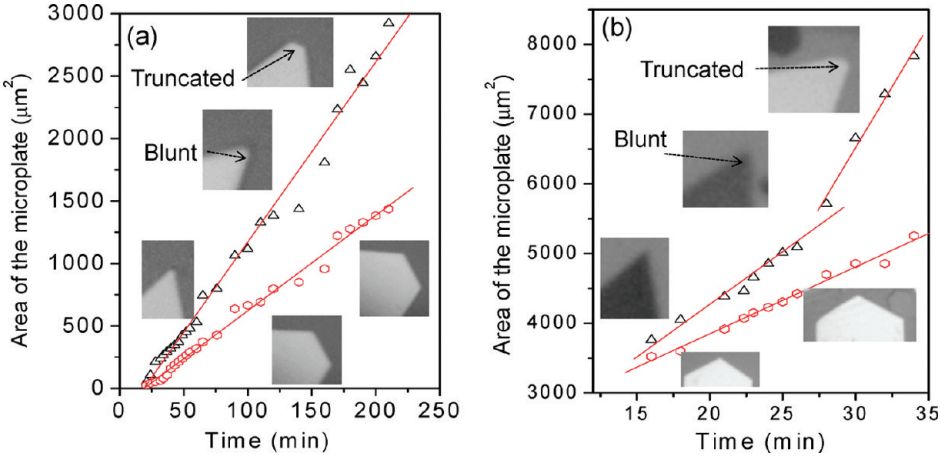

Figure 9. Area of the triangular and hexagonal microplates versus the thermolysis time at (a) 130 °C and (b) 180 °C. The $(AuCl_4)^-$-ToABr precursor is taken in the ratio of 1:4.4. The deviation from the slope is the point of initiation of bluntness of the corner of the triangular microplates, followed by truncation at later stages. Please note that the darker contrast for the initial triangular microplates shown in panel b is because the triangle is not exactly perpendicular to the incident beam.

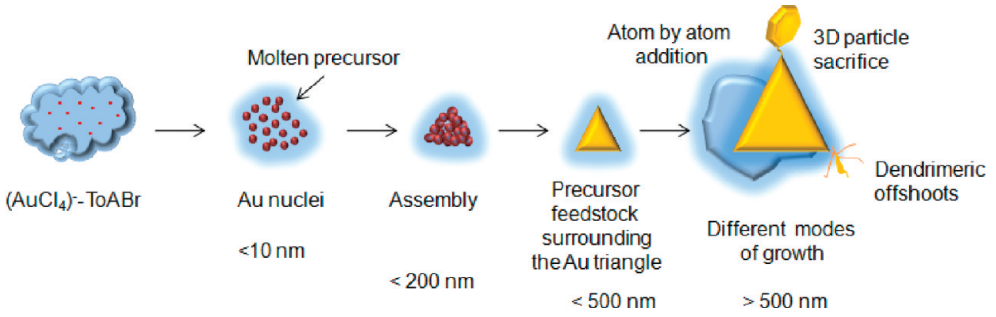

Figure 10. A schematic showing various growth modes, along with the relevant length scales.

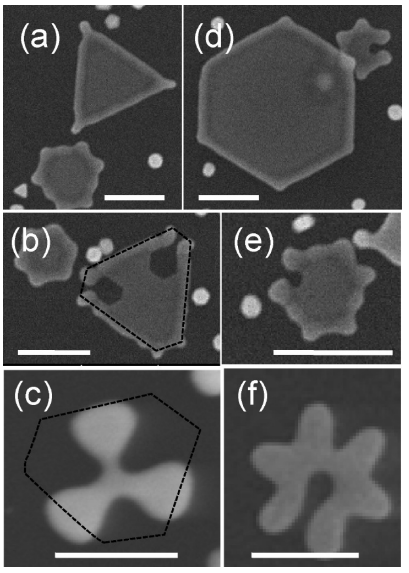

Figure 11. SEM images of Au microplates heated to 350 °C in air. Images in a−c correspond to transformations in triangles while d−f are from hexagons. Initial edge thickening (a and d), cracking initiated along the corners (b and e), and final morphology attained (c and f). The dashed outline in b and c stands for the shape of the microplates before heating. Scale bars, 1 μm.

Conclusions

The study has made use of a simple precursor, namely, $(AuCl_4)^-$-ions phase transferred from aqueous medium and stabilized in toluene by tetraoctylammonium bromide (ToABr) in toluene (50 mM), as a ready source of Au for growing large hexagonal and triangular microplates with edge lengths routinely exceeding 100 μm. The synthetic procedure is only a single step, involving thermolysis of a few drops of the precursor on a flat substrate (Si, glass, HOPG, etc.) in air for extended hours. This process is very different from the known methods in the literature which invariably report synthesis in solution. Many experimental parameters such as precursor concentration, temperature, and time have been varied. The optimal conditions for large microplates have been: $AuCl_4^-$/ToABr ratio of 1:4.4 for phase transfer, thermolysis at 130 °C for 24 h. Electron diffraction data obtained in TEM as well as XRD data revealed that each microplate is a well-formed (111) oriented single crystal with no detectable deformation, unlike most reports on microplates. The surface smoothness as measured using profilometry was less than 1 nm. Scanning electron and optical microscopy studies have been performed in situ in real time to study the growth aspects of Au microplates. At synthetic temperature of 130 °C, the precursor is essentially devoid of the solvent (toluene) but remains molten (m.p., 85 °C), through which Au nanoparticles nucleate and grow into rudimentary shapes. These shapes eventually anneal as well as grow into tiny triangles and hexagons, as seen in SEM. There were also some pentagonal prismatic, dodecahedral, and other 3D structures surrounded by a halo of the molten precursor. There were many instances where 3D structures were seen merging with the microplates. Amazingly quite often the plates were held vertical to the substrate surface during the growth even at large sizes, as evidenced by in situ optical microscopy. Upon heating to higher temperatures, the microplate edges thicken due to the flow of the metal from the central region and cracks appear at the vertices. In other words, the microplates behave as single entities with almost no trace of history of the growth. To sum up, three growth modes namely, nucleation and assembly, atom-by-atom addition, and fusion of the 3D particles, can be inferred from this study using real time microscopy.

Acknowledgment. The authors thank Professor C. N. R. Rao for encouragement. Support from DST is acknowledged. The authors acknowledge Professor K. R. Sreenivas for useful discussions. R.B. thanks CSIR for her fellowship.

Supporting Information Available: (1) SEM images of Au microplates formed on various substrates, (2) XRD of $(AuCl_4)^-$-ToABr complex, (3) optical profilometric images of Au microplates, (4) profilometry showing surface roughness, (5) UV−visible absorption spectrum of the Au microplates, and (6) Table S1 showing effect of alkylchain length of tetraalkylammonium bromide on the size of Au microplates. This material is available free of charge via the Internet at http://pubs.acs.org.

References

(1) Sau, T. K.; Rogach, A. L.; Jäckel, F.; Klar, T. A.; Feldmann, J. *Adv. Mater.* **2010**, *22*, 1805–1825.
(2) Watt, J.; Cheong, S.; Toney, M. F.; Ingham, B.; Cookson, J.; Bishop, P. T.; Tilley, R. D. *ACS Nano* **2009**, *4*, 396–402.
(3) Jin, R.; Cao, Y.; Mirkin, C. A.; Kelly, K. L.; Schatz, G. C.; Zheng, J. G. *Science* **2001**, *294*, 1901–1903.
(4) Murphy, C. J.; Sau, T. K.; Gole, A. M.; Orendorff, C. J.; Gao, J.; Gou, L.; Hunyadi, S. E.; Li, T. *J. Phys. Chem. B.* **2005**, *109*, 13857–13870.
(5) Ciou, S. H.; Cao, Y. W.; Huang, H. C.; Su, D. Y.; Huang, C. L. *J. Phys. Chem. C* **2009**, *113*, 9520–9525.
(6) Kasture, M.; Sastry, M.; Prasad, B. L. V. *Chem. Phys. Lett.* **2010**, *484*, 271–275.
(7) Lin, G.; Lu, W.; Cui, W.; Jiang, L. *Cryst. Growth Des.* **2010**, *10*, 1118–1123.
(8) Seo, D.; Yoo, C. I.; Chung, I. S.; Park, S. M.; Ryu, S.; Song, H. *J. Phys. Chem. C* **2008**, *112*, 2469–2475.
(9) Zhang, J.; Liu, H.; Wang, Z.; Ming, N. *App. Phys. Lett.* **2007**, *91*, 133112–3.
(10) Kim, D. Y.; Im, S. H.; Park, O. O. *Cryst. Growth Des.* **2010**, *10*, 3321–3323.

(11) Chen, H. M.; Liu, R.-S.; Tsai, D. P. *Cryst. Growth Des.* **2009**, *9*, 2079–2087.
(12) Wu, H.-L.; Chen, C.-H.; Huang, M. H. *Chem. Mater.* **2008**, *21*, 110–114.
(13) Nalbant Esenturk, E.; Hight Walker, A. R. *J. Raman Spectrosc.* **2009**, *40*, 86–91.
(14) Lofton, C.; Sigmund, W. *Adv. Funct. Mater.* **2005**, *15*, 1197–1208.
(15) Murayama, H.; Hashimoto, N.; Tanaka, H. *J. Phys. Conf. Ser.* **2009**, *190*, 012132.
(16) Cao, L.; Zhu, T.; Liu, Z. *J. Colloid Interface Sci.* **2006**, *293*, 69–76.
(17) Rocha, T. C. R.; Sato, F.; Dantas, S. O.; GalvaÌfo, D. S.; Zanchet, D. *J. Phys. Chem. C* **2009**, *113*, 11976–11979.
(18) Wang, D. J.; Imae, T. *Chem. Lett.* **2006**, *35*, 1152–1153.
(19) Bai, X.; Zheng, L.; Li, N.; Dong, B.; Liu, H. *Cryst. Growth Des.* **2008**, *8*, 3840–3846.
(20) Yang, S.; Wang, Y.; Wang, Q.; Zhang, R.; Yang, Z.; Guo, Y.; Ding, B. *Cryst. Growth Des.* **2007**, *7*, 2258–2261.
(21) Radha, B.; Arif, M.; Datta, R.; Kundu, T. K.; Kulkarni, G. U. *Nano Res.* **2010**, *3*, 738–747.
(22) Mathias, B.; Merryl, W.; Donald, B.; David, J. S.; Robin, W. *J. Chem. Soc., Chem. Comm.* **1994**, *7*, 801–802.
(23) Wang, C.; Kan, C.; Zhu, J.; Zeng, X.; Wang, X.; Li, H.; Shi, D. *J. Nanomater.* **2010**, *2010*, 969030.
(24) John, N. S.; Thomas, P. J.; Kulkarni, G. U. *J. Phys. Chem. B* **2003**, *107*, 11376–11381.
(25) Xie, J.; Lee, J. Y.; Wang, D. I. C. *J. Phys. Chem. C* **2007**, *111*, 10226–10232.
(26) Jiang, P.; Zhou, J.-J.; Li, R.; Gao, Y.; Sun, T. L.; Zhao, X.-W.; Xiang, Y. J.; Xie, S. S. *J. Nanopart. Res.* **2006**, *8*, 927–934.
(27) Yukselici, M. H. *J. Phys. Cond. Matt.* **2002**, *14*, 1153–1162.
(28) Huang, W.-L.; Chen, C.-H.; Huang, M. H. *J. Phys. Chem. C* **2007**, *111*, 2533–2538.
(29) Xiong, Y.; Washio, I.; Chen, J.; Cai, H.; Li, Z. Y.; Xia, Y. *Langmuir* **2006**, *22*, 8563–8570.
(30) Kan, C.; Wang, G.; Zhu, X.; Li, C.; Cao, B. *App. Phys. Lett.* **2006**, *88*, 071904–3.